Research Article | Vol. 27, No. 19 / 16 September 2019 / Optics Express 26369

Optics EXPRESS

3D conical helix metamaterial–based isotropic broadband perfect light absorber

RENILKUMAR MUDACHATHI[1,2] AND TAKUO TANAKA[2,3,4,*]

[1] Dept. of Physics and Nanotechnology, SRM Institute of Science and Technology, Kattangulathur 603 203, India
[2] Metamaterials Laboratory, RIKEN Cluster for Pioneering Research, Wako 351-0198, Japan
[3] Innovative Photon Manipulation Research Team, RIKEN Center for Advanced Photonics, RIKEN, Wako 351-0198, Japan
[4] Institute of Post-LED Photonics, Tokushima University, Tokushima, Japan
[*] t-tanaka@riken.jp

Abstract: We present the design and fabrication of an isotropic broadband perfect light absorber in the near-infrared range using 3D metamaterials with a single resonator in the unit cell. The metamaterial resonator is comprised of a gold conical helix supported on a silicon pillar with back reflector realized on a silicon substrate. Simulations and experiments have demonstrated that the proposed absorber achieves a broad absorption band of more than 3 μm in the 1.5–4.5 μm wavelength range with an average absorbance of more than 90%. The numerical and experimental analyses show that the proposed device can provide both incident angle and polarization independent operations, which further widens the application prospects of our device.

1. Introduction

Thin broadband optical absorbers have many potential applications in sensing, light detection, IR camouflaging, energy harvesting and communication technologies. Plasmonic nanostructures have been extensively studied for light absorption in many applications like color filters [1,2], structural color printing [3,4], photovoltaics [5,6], photo detection [7], sensing [8,9] and imaging [10]. Most recently, plasmonic nanostructures based multipole oscillators and microcavities have been explored for light ansorption [11–13]. Metamaterials (MMs) on the other hand exhibits tailored response to the electric and magnetic components of the incident electromagnetic radiation. By matching the electric and magnetic parameters in metamaterials, Landy et al has demonstrated the design of a wavelength selective perfect light absorber [14]. Shortly thereafter a lot of efforts have been dedicated for the incorporation of more functionalities like polarization and incident angle independent broadband operations and tunability. A variety of metamaterial geometries have been proposed in which, symmetric structures like square patches, nano disks and circular holes have been explored for polarization independent operations while metal-insulator-metal (MIM) and 3D structures have been explored for incident angle independent operations. Broadband operation has been demonstrated using cascaded multiple resonators of different absorption peaks in the same unit cells and using multilayer structures forming Fabry-Perot (FP) cavity resonances. The design of a metamaterial broadband absorber has been reported with an average absorbance of 50% in the 2–5 μm wavelength range using multiple resonators of different sizes [15]. Lee et al has reported an incident angle and polarization independent broadband light absorber in the visible region using a multi layered semiconductor structure [16]. A broadband metamaterial absorber with an absorbance of more than 75% in the 1.8–2.8 THz frequency range has been proposed using interlaced fishnet layers [17]. Most recently Lei et al has reported a broadband absorber in the visible NIR region with an average absorbance of 97% using plasmonic metamaterials employing MIM FP cavity [18].

#370441 https://doi.org/10.1364/OE.27.026369
Journal © 2019 Received 19 Jun 2019; revised 9 Aug 2019; accepted 10 Aug 2019; published 4 Sep 2019

Optics EXPRESS

In this communication, we present the design of an isotropic broadband perfect light absorber based on conical helix metamaterials for operations in the near IR frequencies and its simple fabrication techniques. Our absorber design is based on a single metamaterial element in the unit cell opposed to the previously reported designs, which consists of multiple resonators of different absorption peaks in the regular intervals of wavelengths [19,20] and multi layers [21,22] to realize broadband operation. The incorporation of multiple resonators of varying geometry in a single unit cell results in to weak light absorption as the effective number density of individual resonators decreases with increasing number of resonator types. As we reported recently, the total light absorption by an MM based absorber is determined by the number density of metamaterial resonators and maximum absorption can be achieved for number densities with minimum inter resonator interactions [23]. In the present absorber design only one resonator type with broadband response is included in the unit cell, which simultaneously ensures sufficient number density to achieve maximum light absorption, and we reported an average experimental absorbance of more than 90% for a broad spectrum of 3 μm in the 1.5–4.5 μm wavelength range, which is of importance due to the fact that many molecules possess vibrational absorption in this range of wavelengths.

2. Design and fabrication

Helical MMs have been studied for their broad electromagnetic response to circularly polarized light [24]. It is also reported that left circularly polarized (LCP) light interacts with left handed helix and right circularly polarized light interacts with right handed helix, and hence the polarization independent operation requires a combined structure of both left and right handed helices in the unit cell. Various designs of broadband absorbers have been proposed using this helical MMs with combined left and right handed helices for polarization independent operation [25,26], but their practical implementation proved to be difficult. Here we present the design of a conical helix MM (CHMM) with single strand showing broadband response to unpolarized electromagnetic radiation. Further, we propose a simple design of an isotropic broadband absorber based on this conical helix MMs and demonstrated its fabrication using residual stress induced bending of thin metal strips. The schematics of the broadband absorber based on CHMM and its single unit cell are shown in the Fig. 1(a) with geometrical dimensions.

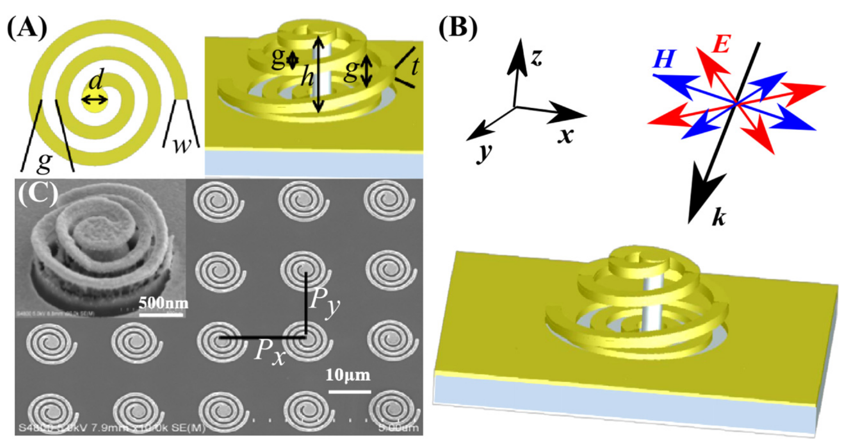

Fig. 1. Geometry of the conical helix metamaterials and its SEM images. (a) Schematics of the conical helix with anchor diameter d, strip width w, inter strip gap g, strip thickness t and pillar height h. (b) Schematic showing the polarization independent broadband response of the CHMM to the incident light. (c) SEM images of the fabricated structures arranged in the 2D lattice with equal periodicities in both directions (tilted image is shown in the inset).

Optics EXPRESS

The perfect light absorber is essentially a quasi-MIM structure comprising of a top CHMM supported by silicon pillar with a perforated back reflector on a silicon substrate. The CHMM and the back reflectors are realized using gold. The inter strip gap g is slightly broadened from top to bottom as the 2D spiral transforms into the conical helix structure as depicted in the 3D schematics shown in Fig. 1(a) and the tilted SEM image in the inset of Fig. 1(c). The structures are arranged in a square lattice with periodicities P_x and P_y in the x and y directions respectively as shown in the SEM image in Fig. 1(c). The fabrication process steps are detailed in Fig. 2. The 2D pattern has been generated and transferred on to a pristine silicon substrate using electron beam lithography and thermal evaporation of 45 nm thick gold films followed by liftoff. The exposed silicon is etched in two steps to realize the CHMM using reactive ion etching (RIE). In the first step a deep anisotropic etching was performed to obtain a deep trench of depth more than 500 nm, which determines the height of the pillar and ultimately the height of the conical helix, as depicted in the step *v*. Followed to the anisotropic RIE an isotropic RIE was performed to release the spiral structure as depicted in the step *vi*, which will slightly increase the pillar height also. Finally, 45 nm thick gold was again deposited on the released spiral structure transforming it in to a conical helix shape as shown in the step *vii*.

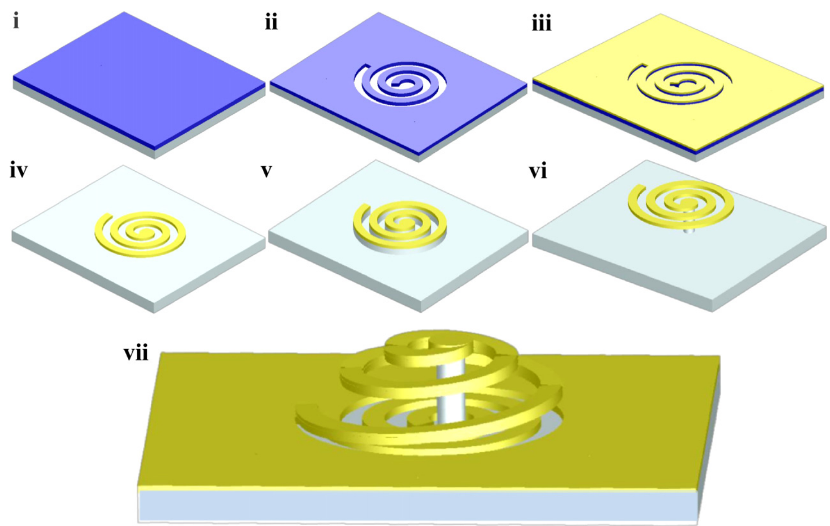

Fig. 2. Fabrication process steps of CHMM comprising of (i) electron beam lithography, (ii) pattern transfer on to resist layer, (iii) thermal evaporation of 45 nm thick Au layer, (iv) liftoff process, (v) anisotropic RIE, (vi) isotropic RIE and (vii) thermal evaporation of 45 nm thick Au layer. The 2D spiral structure transforms in to 3D conical helix by bending the suspended spiral due to the compressive residual stress in the second layer of Au.

The physical mechanism of this structural deformation is the residual stress induced bending of thermally evaporated thin metal strips. 3D split ring resonators based MMs have already been realized by exploiting residual tensile stress in the thermally evaporated metal thin films [27,28], which results in to a concave bending. Here we introduce residual compressive stress to bend the structures in a convex shape. The compressive stress in the second layer of Au bent down the already released spiral in the second RIE process. The second layer of gold also forms the back reflector which is shadowed by the elevated spiral making it perforated in the shape of the top spiral on the silicon substrate as seen in the 3D schematic and SEM images.

Optics EXPRESS

3. Results and discussion

We have fabricated CHMM with varying periodicity from 1.2 to 1.5 µm to study the inter atomic interactions and its influence on the light absorption. It is found that the light absorbance is maximum for high filling fraction and decreasing with increasing periodicity as shown in the Fig. 3(b). Further we have numerically studied the absorbance by varying the filling fraction of the CHMM in the square lattice. The theoretical analysis was carried out using Lumerical's FDTD solutions in which the dimensions *h, t, w* and *d* were set to 700 nm, 90 nm, 100 nm, and 200 nm, respectively. The gap *g* was defined by the angle at which each ring bent and is made slightly varying from top to bottom to match with the fabricated structures. The theoretical analyses have predicted a decreasing absorbance with decreasing filling fraction as shown in the Fig. 3(a). This is due to the decreasing number density of the resonators in a given area of the CHMM systems [23].

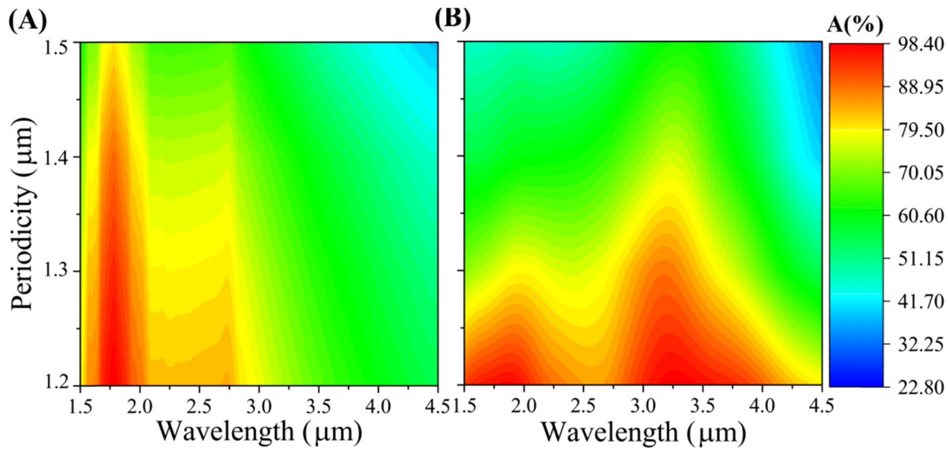

Fig. 3. Absorbance of the CHMM based perfect light absorber for varying lattice parameters. (a) Simulated and (b) measured absorbance with respect to varying periodicity in x and y directions. The periodicity in x and y directions varied equally.

We predicted the maximum light absorption for a filling fraction of 0.83 with equal separation between the resonators in both x and y directions. The minimum separation of 200 nm at which the CHMM has maximum absorbance is set by the fabrication tolerance. We fabricated structures with varying inter resonator separation from 200 to 500 nm and measured the reflectance and transmittance using an FTIR microspectroscope (FT/IR-6300FV, Jasco) in the 1500–4500 nm wavelength range. Both in the experiment and simulation, unpolarized light is incident normally on to the sample. The structures show a flat transmission of near zero value due to the presence of perforated back reflector. The experimentally calculated absorbance of the structures using the formula $A(\lambda) = 1 - (R(\lambda) + T(\lambda))$ for varying inter resonator separation is shown in the Fig. 3(b).

Figure 4(a) shows a comparison between the simulated and measured absorbance of the structures with 200 nm separation. The structure has broad absorption of more than 3 µm in the mid IR region. The structure has two major absorption peaks one at around 1.8 µm and the other at around 3.25 µm with a maximum absorbance of more than 98%. The CHMM has an average absorbance of more than 90% for over a bandwidth of 3 µm, which is comparable to any other literature values [29,30]. The slight mismatch between the calculated and measured absorbance seen in the Fig. 4(a) might be due to the geometrical variation between the theoretical model and the actual device, especially the gap between rings (*g*) and pillar height (*h*). We have studied three different geometries as shown in the Fig. 4(b) to understand the physical origin of the broadband operation. The corresponding SEM images of each geometry are shown in

Optics EXPRESS

the inset. The released and unreleased spirals marked (ii) and (iii) respectively in the Fig. 4(b) show distinct peaks, but in the case of conical helix marked as (i) shows overlapped resonant modes giving a broad absorption spectrum. The mechanism behind the broad absorption is the overlapping of closely spaced higher order modes, which are resulted from the circulating currents in the rings forming the CHMM [24]. The current density (J_x) plot for the structure with six half rings shown in the Fig. 5 clarifies the existence of multiple resonant modes and its overlapping to from broad absorption spectrum.

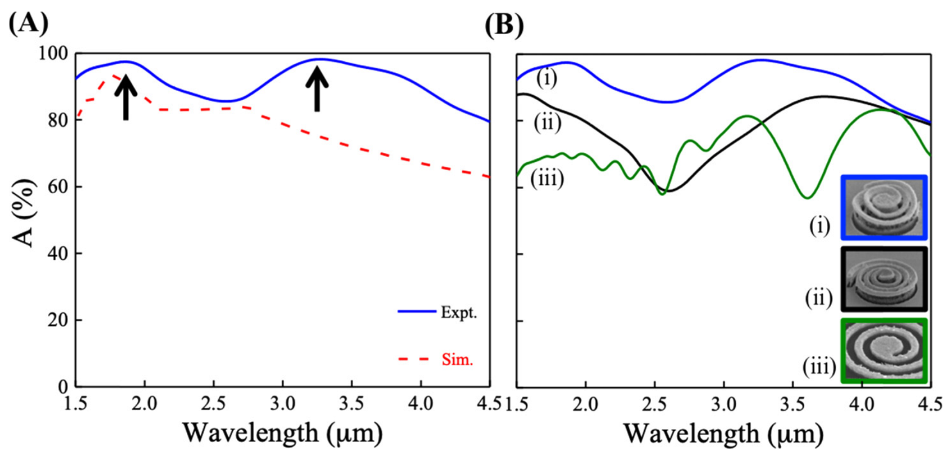

Fig. 4. Absorption spectrum of the CHMM for 200 nm separation. (a) Comparison between measured (solid blue line) and calculated (dotted red line) percentage absorption in the 1.5–4.5 µm wavelength range. (b) Comparison of the percentage absorption by different geometries (i) conical helix, (ii) released spiral and (iii) unreleased spiral for the same wavelength range.

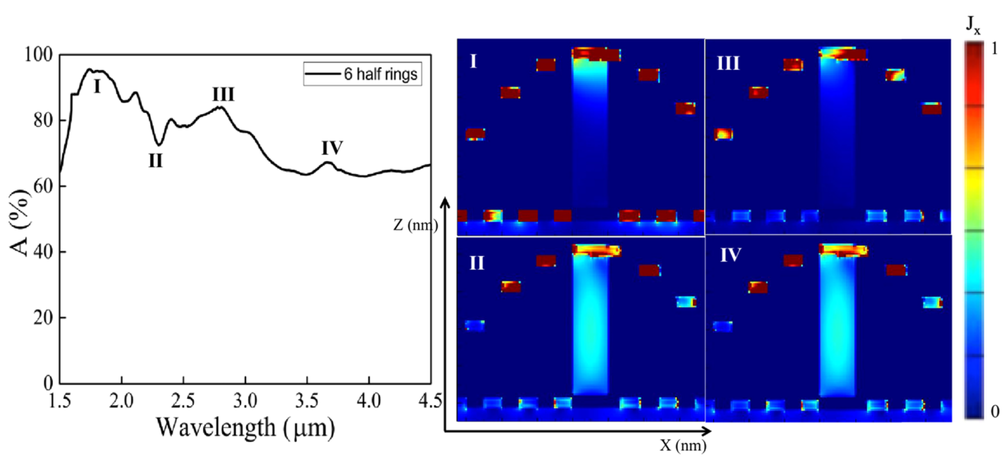

Fig. 5. The absorption spectrum of the CHMM with 6 half rings (left) and the calculated current densities for peak wavelengths 1750nm, 2250 nm, 2800 nm and 3600 nm represented as I, II, III and IV respectively (right)

The spectrum of the structure is shown in the left and the current densities are calculated for the wavelengths 1750nm, 2250 nm, 2800 nm and 3600 nm represented as I, II, III and IV respectively in the right side of the Fig. 5.

In the proposed CHMM the broadband operation is determined by the conical shape of the metamaterial resonator, which can be viewed as a stack of ascending rings. The conical shape formation in the fabricated structures is gradual which resulted in to the flat absorption spectrum as shown in the Fig. 4(a). We have studied the dependence of light absorption on the degree of conical shape by changing the angle of bent (2θ) between successive half rings in the computer model and the schematic is depicted in the inset of Fig. 6(a). It is found that the individual peaks merge together to form a broad flat spectrum as the spiral structure ($2\theta = 0°$) evolved in to a conical helix. We got a maximum absorption for an angle of $2\theta = 5°$ as detailed in the Fig. 6(a).

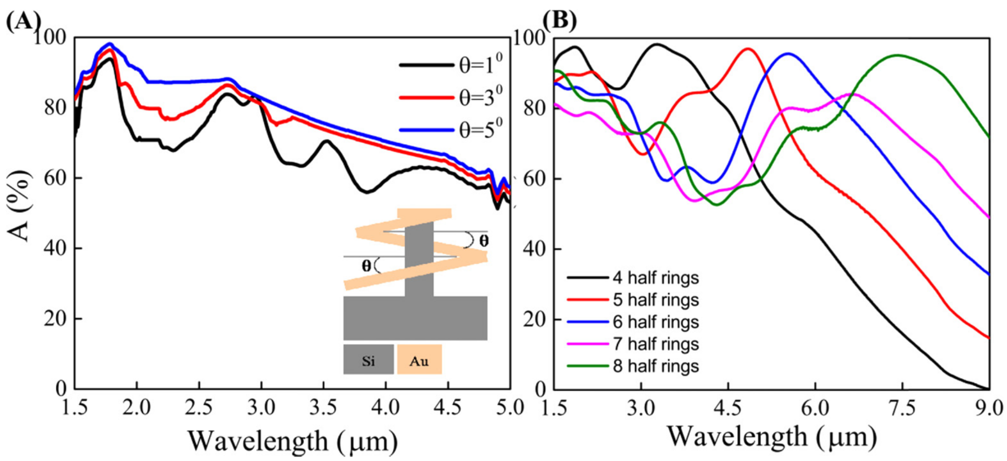

Fig. 6. (a) The dependence of absorption and spectral shape on the degree of conical shape, which is determined by θ, the inset shows the schematic of the angle of bent between successive half rings (b) and the absorption spectra for CHMMs with varying number of half rings

CHMM with varying number of rings have been fabricated to study its dependence on light absorption. We have considered number of half rings that make the CHMM. The result reveals that more number of rings reduces the absorbance. This comes from the fact that the resonator size increases with increasing number of rings, which in turn reduces the number density of the resonator. Therefore, the maximum absorption is obtained for the CHMM with four half rings as shown in the Fig. 6(b). It can also be seen from the Fig. 6(b) that the resonances shift to longer wavelength for increasing number of rings.

Finally we have studied the dependence of polarization and incident angles on the absorption spectrum. We calculated the absorption spectrum of the CHMM with 4 half rings for varying angles of incidence from 0° to 60° and depicted in the Fig. 7(a). It is seen from this graph that the absorption is invariant up to an angle of 35° and then started to decrease slightly with increasing incident angle. It is also evident that the structure shows broadband absorption of 60% up to an incident angle of 60°. Further, we measured the absorption spectrum of the CHMM for varying polarization angle from 0° to 90° by using a linear polarizer, and is shown in the Fig. 7(b). It is clear from this plot that the spectrum is polarization angle insensitive.

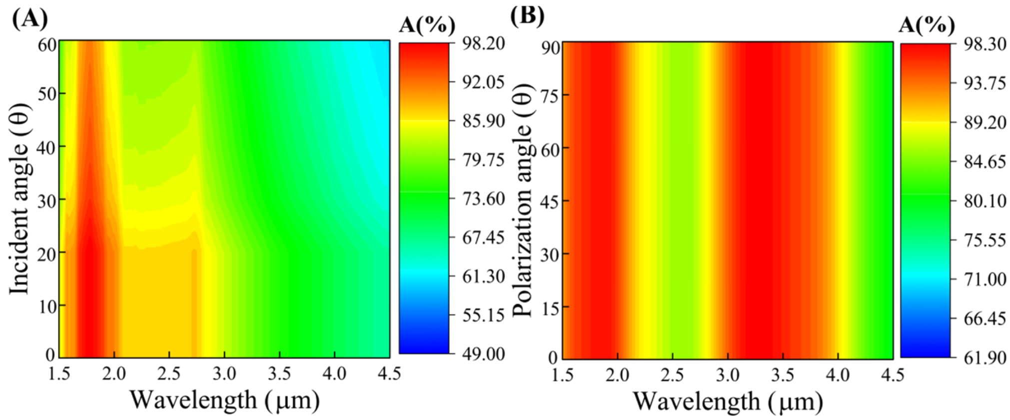

Fig. 7. Isotropic operation of the CHMM. (a) Calculated absorption spectrum for different angles of incidence. (b) Measured absorption spectrum for different polarization angles.

4. Conclusions

In conclusion, we designed and fabricated an isotropic broadband perfect light absorber based on conical helix metamaterials. We demonstrated polarization independent broadband operation with a single helix resonator in the metamaterial unit cell in contrast with other designs, which employed multiple resonators of different absorption peaks and polarization response. We further demonstrated a simple fabrication technique based on residual stress induced bending of thin metal strips to fabricate 3D metamaterial structures. Compressive type residual stress is induced in the deposited thin metal strip by controlling the thermal evaporation parameters, which bent the suspended spiral in to a conical helix shape. An experimental absorption of more than 90% over a broad wavelength range of 3 µm from 1.5 µm to 4.5 µm is achieved with our device, which will find applications in background suppressed SEIRA, IR camouflaging and solar harvesting to name a few. Besides that, the CHMM is polarization insensitive in comparison with helical MMs, which are sensitive to circularly polarized light. We have theoretically studied the effect of incident angle on the absorption spectrum and shown the conical shape of our device ensures incident angle independent operation up to an angle of 35°.

Acknowledgments

The work made use of the RIKEN's nano fabrication facility in the emergence matter science department and simulation and characterization facilities in Metamaterials laboratory.

References

1. G. Si, Y. Zhao, J. Lv, M. Lu, F. Wang, H. Liu, N. Xiang, T. J. Huang, A. J. Danner, and J. Teng, "Reflective plasmonic color filters based on lithographically patterned silver nanorod arrays," Nanoscale **5**(14), 6243–6248 (2013).
2. T. W. Ebbesen, H. J. Lezec, H. F. Ghaemi, T. Thio, and P. A. Wolff, "Extraordinary optical transmission through sub-wavelength hole arrays," Nature **391**(6668), 667–669 (1998).
3. K. Kumar, H. Duan, R. S. Hegde, S. C. W. Koh, J. N. Wei, and J. K. W. Yang, "Printing colour at the optical diffraction limit," Nat. Nanotechnol. **7**(9), 557–561 (2012).
4. R. Mudachathi and T. Tanaka, "Up Scalable Full Colour Plasmonic Pixels with Controllable Hue, Brightness and Saturation," Sci. Rep. **7**(1), 1199 (2017).
5. Y. Wang, T. Sun, T. Paudel, Y. Zhang, Z. Ren, and K. Kempa, "Metamaterial-plasmonic absorber structure for high efficiency amorphous silicon solar cells," Nano Lett. **12**(1), 440–445 (2012).
6. R. Mudachathi and T. Tanaka, "Broadband plasmonic perfect light absorber in the visible spectrum for solar cell applications," Adv. Nat. Sci.: Nanosci. Nanotechnol. **9**(1), 015010 (2018).
7. I. J. Luxmoore, P. Q. Liu, P. Li, J. Faist, and G. R. Nash, "Graphene–metamaterial photodetectors for integrated infrared sensing," ACS Photonics **3**(6), 936–941 (2016).

Optics EXPRESS

8. K. M. Mayer and J. H. Hafner, "Localized surface plasmon resonance sensors," Chem. Rev. **111**(6), 3828–3857 (2011).
9. A. Ishikawa and T. Tanaka, "Metamaterial absorbers for infrared detection of molecular self-assembled monolayers," Sci. Rep. **5**(1), 12570 (2015).
10. R. Y. He, C. Y. Lin, Y. D. Su, K. C. Chiu, N. S. Chang, H. L. Wu, and S. J. Chen, "Imaging live cell membranes via surface plasmon-enhanced fluorescence and phase microscopy," Opt. Express **18**(4), 3649–3659 (2010).
11. L. Chen, N. Xu, L. Singh, T. Cui, R. Singh, Y. Zhu, and W. Zhang, "Defect-Induced Fano Resonances in Corrugated Plasmonic Metamaterials," Adv. Opt. Mater. **5**(8), 1600960 (2017).
12. L. Chen, L. Deng-gao, G. Xu-guang, Z. Jia-yu, Z. Yi-ming, and Z. Song-lin, "Terahertz time-domain spectroscopy and micro-cavity components for probing samples: a review," Frontiers Inf. Technol. Electronic Eng. **20**(5), 591–607 (2019).
13. L. Chen, Y. Wei, X. F. Zang, Y. M. Zhu, and S. L. Zhuang, "Excitation of dark multipolar plasmonic resonances at terahertz frequencies," Sci. Rep. **6**(1), 22027 (2016).
14. N. I. Landy, S. Sajuyigbe, J. J. Mock, D. R. Smith, and W. J. Padilla, "Perfect metamaterial absorber," Phys. Rev. Lett. **100**(20), 207402 (2008).
15. W. Ma, Y. Wen, and X. Yu, "Broadband metamaterial absorber at mid-infrared using multiplexed cross resonators," Opt. Express **21**(25), 30724–30730 (2013).
16. K. T. Lee, C. Ji, and L. J. Guo, "Wide-angle, polarization-independent ultrathin broadband visible absorbers," Appl. Phys. Lett. **108**(3), 031107 (2016).
17. S. Tan, F. Yan, N. Xu, J. Zheng, W. Wang, and W. Zhang, "Broadband terahertz metamaterial absorber with two interlaced fishnet layers," AIP Adv. **8**(2), 025020 (2018).
18. L. Lei, S. Li, H. Huang, K. Tao, and P. Xu, "Ultra-broadband absorber from visible to near-infrared using plasmonic metamaterial," Opt. Express **26**(5), 5686–5693 (2018).
19. S. Gu, B. Su, and X. Zhao, "Planar isotropic broadband metamaterial absorber," J. Appl. Phys. **114**(16), 163702 (2013).
20. J. Wang, W. Zhang, M. Zhu, K. Yi, and J. Shao, "Broadband perfect absorber with titanium nitride nano-disk array," Plasmonics **10**(6), 1473–1478 (2015).
21. F. Ding, Y. Jin, B. Li, H. Cheng, L. Mo, and S. He, "Ultrabroadband strong light absorption based on thin multilayered metamaterials," Laser Photonics Rev. **8**(6), 946–953 (2014).
22. M. K. Hedayati, M. Javaherirahim, B. Mozooni, R. Abdelaziz, A. Tavassolizadeh, V. S. Kiran Chakravadhanula, V. Zaporojtchenko, T. Strunkus, F. Faupel, and M. Elbahri, "Design of a Perfect Black Absorber at Visible Frequencies Using Plasmonic Metamaterials," Adv. Mater. **23**(45), 5410–5414 (2011).
23. R. Mudachathi, Y. Moritake, and T. Tanaka, "Controlling coulomb interactions in infrared stereometamaterials for unity light absorption," Appl. Phys. Lett. **112**(20), 201107 (2018).
24. J. K. Gansel, M. Thiel, M. S. Rill, M. Decker, K. Bade, V. Saile, G. V. Freymann, S. Linden, and M. Wegener, "Gold helix photonic metamaterial as broadband circular polarizer," Science **325**(5947), 1513–1515 (2009).
25. S. Agarwal and Y. K. Prajapati, "Broadband and polarization-insensitive helix metamaterial absorber using graphene for terahertz region," Appl. Phys. A **122**(6), 561 (2016).
26. Z. Lu, M. Zhao, Z. Y. Yang, L. Wu, and P. Zhang, "Helical Metamaterial Absorbers: broadband and polarization-independent in optical region," J. Lightwave Technol. **31**(16), 2762–2768 (2013).
27. C. C. Chen, A. Ishikawa, Y. H. Tang, M. H. Shiao, D. P. Tsai, and T. Tanaka, "Uniaxial-isotropic metamaterials by three-dimensional split-ring resonators," Adv. Opt. Mater. **3**(1), 44–48 (2015).
28. Y. Moritake and T. Tanaka, "Controlling bi-anisotropy in infrared metamaterials using three-dimensional split-ring-resonators for purely magnetic resonance," Sci. Rep. **7**(1), 6726 (2017).
29. N. T. Q. Hoa, P. H. Lam, and P. D. Tung, "Wide-angle and polarization independent broadband microwave metamaterial absorber," Microw. Opt. Technol. Lett. **59**(5), 1157–1161 (2017).
30. F. Ding, J. Dai, Y. Chen, J. Zhu, Y. Jin, and S. I. Bozhevolnyi, "Broadband near-infrared metamaterial absorbers utilizing highly lossy metals," Sci. Rep. **6**(1), 39445 (2016).